Substitution effect of Y³⁺ ions on the structural, magnetic and electrical properties of cobalt ferrite nanoparticles

(Efeito da substituição de íons de Y³⁺ nas propriedades estruturais, magnéticas e elétricas das nanopartículas de ferrita de cobalto)

S. S. Satpute¹, S. R. Wadgane², K. Desai³, D. R. Mane⁴, R. H. Kadam¹*

¹*Shrikrishna Mahavidyalaya, Materials Science Research Laboratory, Gunjoti, Osmanabad (M.S.), India*
²*Dhole Patil College of Engineering Wagholi, Physics Department, Pune (M.S.), India*
³*ASC College, Physics Department, Kille Dharur, Dist. Beed (M.S.), India*
⁴*Government of Maharashtra, Department of Higher Education, Central Building, Pune (M.S.), India*

Abstract

Y³⁺-doped cobalt ferrite nanoparticles, $CoY_xFe_{2-x}O_4$ (x=0.00, 0.05, 0.10, 0.15), were synthesized using the sol-gel auto-combustion technique. Single-phase cubic spinel structure was confirmed by the X-ray diffraction technique. The lattice parameter increased with the increase of Y³⁺ content in the cobalt ferrite and varied from 8.3876 to 8.4271 Å. FE-SEM images showed that the samples had distinct crystalline nanoparticles of spherical shape with small agglomeration. EDAX results showed good agreement with the particularized composition. Magnetic measurement using a vibrating sample magnetometer (VSM) recorded a reduction in saturation magnetization (M_s) and coercivity (H_c) by Y³⁺ substitution. The values of M_s and H_c ranged from 66.61 to 17.52 emu/g and 1168.9 to 801.9 Oe, respectively. The electrical properties of Y³⁺-substituted cobalt ferrite were studied by measuring the dielectric constant and loss. With increasing frequency, the value of the dielectric constant decreased, as a natural behavior of the ferrite material.

Keywords: sol-gel, XRD, VSM, dielectric constant.

Resumo

Nanopartículas de ferrita de cobalto dopada com Y³⁺, $CoY_xFe_{2-x}O_4$ (x=0,00, 0,05, 0,10, 0,15), foram sintetizadas usando a técnica de autocombustão sol-gel. A estrutura de espinélio cúbico monofásica foi confirmada pela técnica de difração de raios X. O parâmetro da rede aumentou com o aumento do teor de Y³⁺ na ferrita de cobalto e variou de 8,3876 para 8,4271 Å. Imagens de MEV mostraram que as amostras possuíram nanopartículas cristalinas distintas de forma esférica com pequena aglomeração. Os resultados de EDAX mostraram boa concordância com a composição especificada. A medição magnética usando o magnetômetro de amostra vibrante (VSM) registrou uma redução na magnetização de saturação (M_s) e coercividade (H_c) pela substituição de Y³⁺. Os valores de M_s e H_c variaram de 66,61 a 17,52 emu/g e 1168,9 a 801,9 Oe, respectivamente. As propriedades elétricas da ferrita de cobalto substituído com Y³⁺ foram estudadas por meio da medição de constante e perda dielétrica. Com o aumento da frequência o valor da constante dielétrica diminuiu, conforme comportamento natural da ferrita.

***Palavras-chave**: sol-gel, DRX, VSM, constante dielétrica.*

INTRODUCTION

The scientific community shows a prominent interest in the various properties of magnetic materials with their nanoscale dimensions. The nanoscale crystallites have a high surface to volume ratio leading to magnetic properties different from those of bulk particles and show large-scale applications in permanent magnets, magnetic drug delivery, microwave devices, high-density information storage, etc. [1]. Method of preparation, amount and type of dopant affect their structural, electrical and magnetic properties [2]. The structural and magnetic properties of spinel ferrite also depend on magnetic interaction and cation distribution in the two sub-lattices i.e. tetrahedral (A) and octahedral (B) sites [3, 4]. Among all nano-ferrites, cobalt ferrite is one of the challenging materials for high-density recording media because of its high coercivity (H_c), moderate saturation magnetization (M_s), chemical stability, and mechanical hardness. For high-density recording media, the small grain size is expressly required because it results in the lower media noise for light scattering at grain boundaries [5]. Cobalt ferrite has an inverse spinel structure with Co²⁺ ions in the octahedral (B) sites and Fe³⁺ ions equally distributed between tetrahedral (A) and octahedral (B) sites [6, 7].

Various chemical reactions are generally used to produce nanocrystalline ferrite powders rather than a solid-state reaction. One of the most well-known nonconventional

synthesis methods is the sol-gel auto-combustion method, which is a promising technique for preparing homogenous ferrite powder samples with nanocrystalline size. Many researchers have studied cobalt ferrite with the substitution of different rare earth metal ions [8]. Singhal et al. [9] reported that saturation magnetization and coercivity decrease by substituting for Cr^{3+} cation; there is a slight decrease in the value of lattice constant from 8.3837 to 8.3736 Å and the crystallite size ranged from 39.36 to 43.02 nm. Jacobo and Bercoff [10] observed that the dielectric constant decreases with yttrium content, showing a constant behavior in the examined frequency range and exhibiting an increasing trend in the lattice constant from 8.3983 to 8.4033 Å. Pachpinde et al. [11] investigated Pr^{3+}-substituted $CoFe_2O_4$ synthesized by the sol-gel auto-combustion method and concluded that $Pr_xCoFe_{2-x}O_4$ nanosized ferrite samples show the formation of a cubic spinel crystal structure. This study [11] also clarifies that the variation in the theoretical and experimental lattice parameter is in good agreement with each other.

The addition of non-magnetic Y^{3+} ion in cobalt ferrite strongly affects the magnetic properties. Also, yttrium ion enters the octahedral site of the lattice which increases the inversion parameter of cobalt ferrite. Even so, to the best of authors' information, there are no records available in the literature with respect to the substitution of Y^{3+} ion in spinel cobalt ferrite manufactured by the sol-gel auto-combustion technique and, thus, its structural, magnetic and dielectric properties were studied at room temperature.

EXPERIMENTAL

Materials: appropriate proportions of metal nitrates were used to prepare nanosized crystals of Y^{3+}-substituted cobalt ferrite by the sol-gel auto-combustion method having the general chemical formula $CoY_xFe_{2-x}O_4$ (x= 0.00, 0.05, 0.10, 0.15). The starting reagents of analytical grade yttrium nitrate $[Y(NO_3)_3.9H_2O]$, ferric nitrate $[Fe(NO_3)_3.9H_2O]$, cobalt nitrate $[CO(NO_3)_3.9H_2O]$ and $C_6H_8O_7.H_2O$ (hydrated citric acid) were used.

Sample preparation: all metal nitrates and citric acid were mixed in appropriate stoichiometric proportions and dissolved in the minimum amount of double distilled water to get a mixed homogeneous solution. Citric acid played an essential role in the segregation and homogenous distribution of metal ions. The present reaction was conducted in an air atmosphere, without the protection of inert gases. The solution was stirred continuously and citric acid was then added into nitrate solution having the molar ratio 1:3. In order to maintain the pH at 7, liquid ammonia was added dropwise in the solution. The obtained solution was put over the hot plate for heating at 100 °C with constant stirring until the solution was converted into a viscous gel. The viscous gel started foaming when all water molecules evaporated from the solution after 3 to 4 h. After that, the gel was placed on a hot plate at 150 °C then the ignition occurred and the fine powder of Y^{3+}-substituted cobalt ferrite was obtained. Finally, the prepared samples were ground with mortar and

pestle for 1-2 h. The samples were finally sintered at 800 °C for 6 h to obtain the final product in the form of crystalline nanoparticles. The uniaxial hydraulic pressure machine was used to make pellets of the as-prepared samples of diameter 10 mm and thickness 1 mm with the addition of PVA as a binder. The prepared pellets were also sintered at 800 °C in a muffle furnace for 4 h.

Characterization: X-ray diffraction technique (Ultima-IV, Rigaku) was used to investigate the structural parameters of prepared samples. X-ray diffraction patterns were recorded at room temperature in the 2θ range 20° to 80° using CuKα radiation (λ=1.5404 Å). The particle morphology of the sample was studied by field emission scanning electron microscope (FE-SEM, JSM-6360, Jeol). The elemental composition of $CoY_xFe_{2-x}O_4$ samples was studied by energy dispersive X-ray analysis (EDAX). The high-resolution transmission electron microscope (HR-TEM) was used to determine particle size and interplanar spacing of the prepared samples. The magnetic properties were examined by vibrating sample magnetometer (VSM) applying a magnetic field of 1.5 tesla at room temperature. The dielectric properties (dielectric constant and dielectric loss) were estimated with the assistance of LCR-Q meter as a function of frequency.

RESULTS AND DISCUSSION

Structural analysis: Fig. 1a shows the X-ray diffraction (XRD) patterns of Y^{3+} ion-substituted $CoY_xFe_{2-x}O_4$ for x=0.00, 0.05, 0.10, 0.15. All the diffraction peaks were fairly matched with standard peaks which confirmed the phase purity of the samples as there were no additional impurity reflection peaks. The broadening of the diffraction peaks confirmed the nanometer size of the crystallite. The formation of cubic structure in the samples had distinct peaks of the crystalline FCC phase, which was verified on the XRD pattern. The ferrite phase was identified by the crystal planes (220), (311), (222), (400), (422), (333), (440) and (533) at 30.12°, 35.48°, 37.11°, 43.12°, 53.55°, 57.06°, 62.65° and 74.16° 2θ angles, respectively, for x=0.0. All peaks were of a cubic unit cell and matched with JCPDS No. 22-1086.
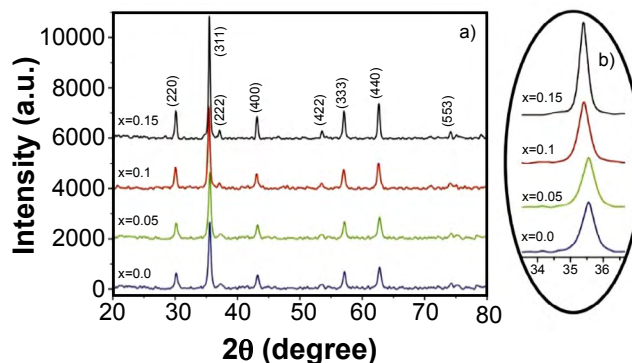

Figure 1: X-ray diffraction patterns of Y^{3+} ion-substituted $CoY_xFe_{2-x}O_4$ for x=0.00, 0.05, 0.10, 0.15 (a) and enlarged view of (311) peaks (b).
[Figura 1: Padrões de difração de raios X de amostras de $CoY_xFe_{2-x}O_4$ para x=0,00, 0,05, 0,10, 0,15 (a) e região ampliada do pico (311) (b).]

The value of the lattice parameter 'a' was calculated from the most intense (311) peak of XRD pattern (Fig. 1b) using the following equation [12]:

$$a = \frac{d_{hkl}}{\sqrt{h^2 + k^2 + l^2}} \qquad (A)$$

where d_{hkl} is the interplanar distance for hkl plane. It was noted that the value of the lattice parameter 'a' increased from 8.3876 to 8.4271 Å with increasing yttrium content in the composition of cobalt ferrite (Table I). It was attributed to the variation in the ionic radii of Y^{3+} (0.9 Å) and Fe^{3+} (0.63 Å) [13]. An expansion of the lattice constant is assumed when the smaller ions are replaced by the larger ions. The average crystallite size was estimated from the most intense peak (311) using Scherrer's formula as discussed elsewhere [14]. The formation of the nanosized particle was confirmed by the value of crystallite size in the nanometer range. It was seen that the crystallite size diminished with an increase in the Y^{3+} substitution in ferrite from 33.71 to 21.57 nm. Similarly, the XRD-derived density of material increased with Y^{3+} concentration in CFO ($CoFe_2O_4$) from 5.2819 to 5.3180 g/cm³ (Table I). The factors like the molecular weight and the lattice constant affect the XRD density of the sample. From our study, it strictly noticed that values of lattice parameter and XRD density showed increasing trends. As XRD density is inversely proportional to the lattice parameter, it should show the opposite behavior, but in the present examination XRD density enhanced with concentration because the molecular weight increased, which overtook the increase in the volume of the unit cell. This behavior of lattice constant and XRD density is in good agreement with the previous literature [15]. It is remarked that the values of the specific surface area increased as the substitution increased [16].

Compositional analysis: for the determination of the chemical composition of the prepared samples, the standard technique EDAX was used. Fig. 2 shows EDAX spectra of Y^{3+} ion-substituted $CoY_xFe_{2-x}O_4$ sintered at 800 °C for 6 h, for the particular samples x=0.0 (Fig. 2a) and x=1.5 (Fig. 2b). The EDAX spectra revealed that all the peaks of their parent elements were present in the samples. The atomic weight percentages of different cations in the prepared samples were observed to be nearly accurate. Fig. 2 confirmed that only O, Fe, Co, and Y were present in prepared samples and did not contain any type of impurities and iron had very high concentration as expected.

Morphological analysis: to investigate the morphology and microstructure, the technique of field emission scanning electron microscopy (FE-SEM) was used. The typical FE-SEM micrographs of the samples x= 0.0 and 0.15 are shown in Fig. 3. FE-SEM micrographs showed that the prepared

Table I - Structural parameters of $CoY_xFe_{2-x}O_4$ samples.
[Tabela I - Parâmetros estruturais de amostras de $CoY_xFe_{2-x}O_4$.]

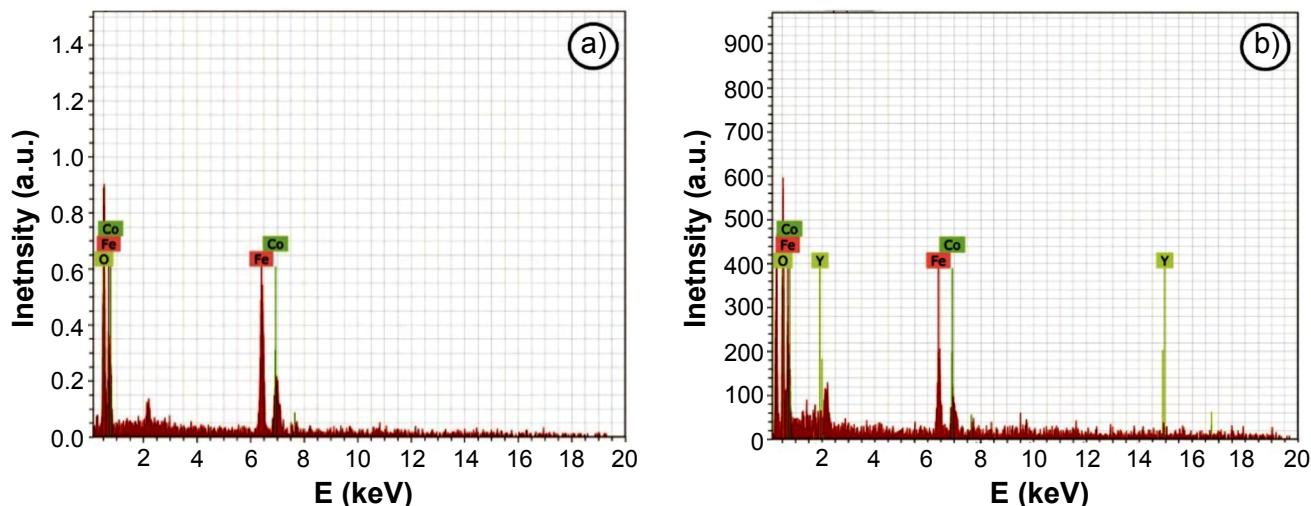| Y^{3+} content, x	d (nm)	a (Å)	ϱ_x (g/cm³)	ϱ_b (g/cm³)	S (m²/g)
0.00	33.71	8.3876	5.2819	3.831	46.45
0.05	25.94	8.4045	5.2871	3.900	59.31
0.10	22.29	8.4126	5.3087	3.950	68.15
0.15	21.57	8.4271	5.3180	3.993	69.65

Figure 2: EDAX spectra for $CoY_xFe_{2-x}O_4$ samples: a) x=0.0; and b) x=0.15.
[Figura 2: Espectros de EDS de amostras de $CoY_xFe_{2-x}O_4$: a) x=0,0; e b) x=0,15.]

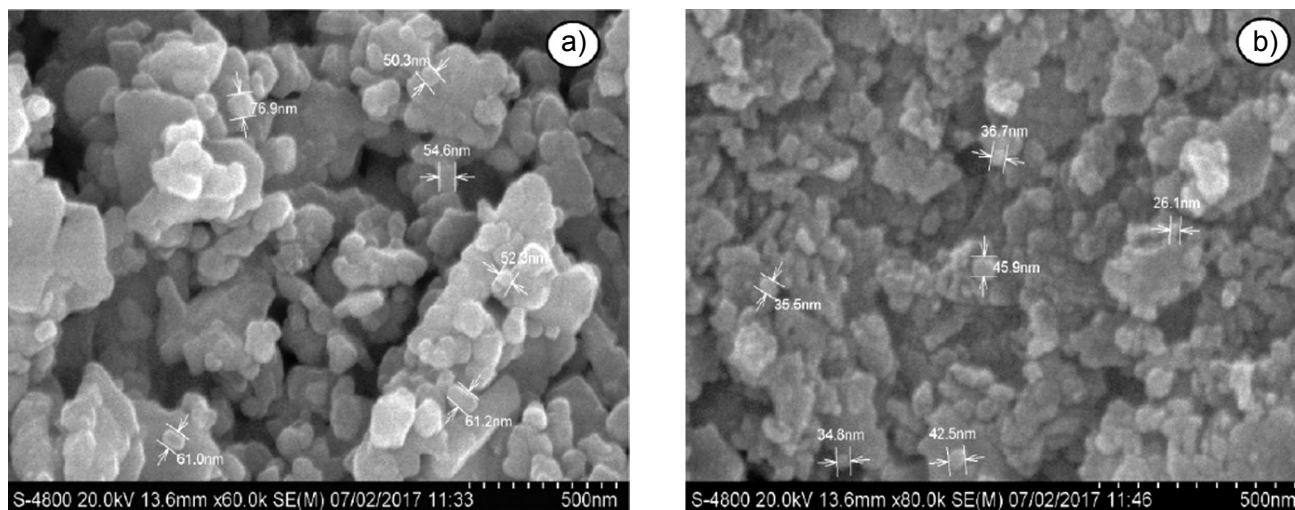Figure 3: FE-SEM micrographs of $CoY_xFe_{2-x}O_4$ samples: a) x=0.0; and b) x=0.15.
[Figura 3: Micrografias de MEV de amostras de $CoY_xFe_{2-x}O_4$: a) x=0,0; e b) x=0,15.]
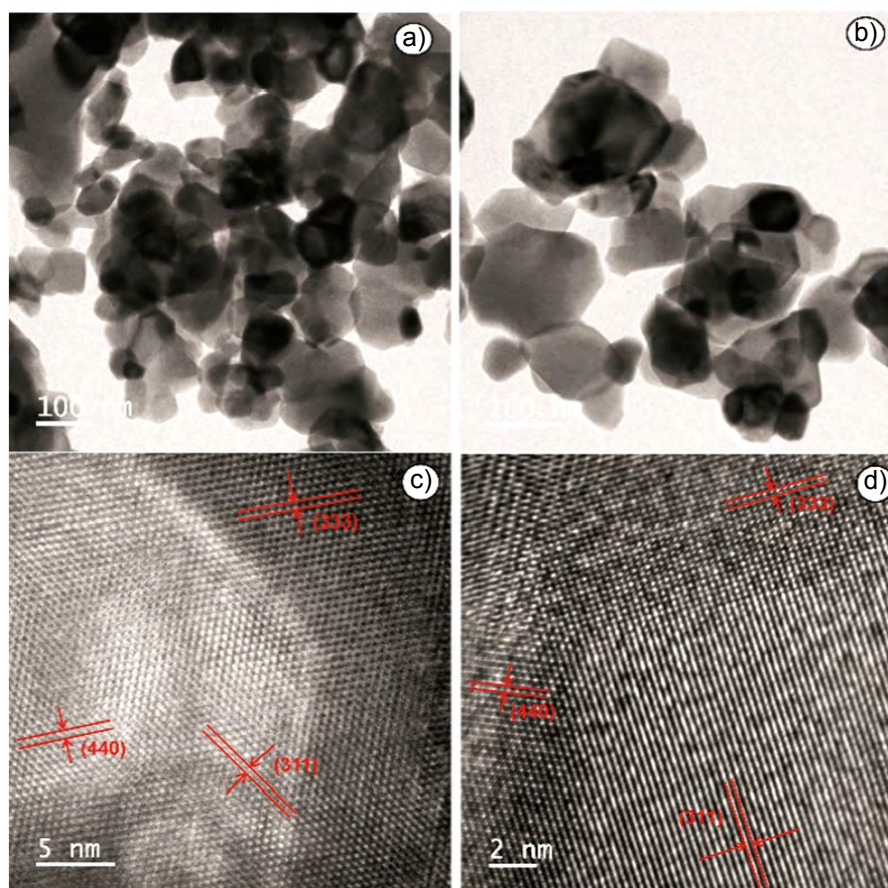

Figure 4: TEM (a,b) and HR-TEM (c,d) images of $CoY_xFe_{2-x}O_4$ samples: a,c) x=0.0; and b,d) x=0.15.
[Figura 4: Imagens de MET (a,b) e MET-AR (c,d) de amostras de $CoY_xFe_{2-x}O_4$: a,c) x=0,0; e b,d) x=0,15.]

samples had sharp crystalline nanosized granular particles of spherical shape with soft agglomeration. The formation of agglomeration was associated with the magnetic exchange interaction within the nanoparticles; because of this, a reasonable boundary between neighboring crystallites was seen. Also, it was noticed that the particles with the substitution of yttrium showed a uniform and finer nanoparticles, which were extra reactive and therefore more agglomerated. Smaller crystallites were consistently observed over the whole region showing excellent grain growth restriction. The magnetic and electrical properties were strongly affected due to the increase in the average grain size of the prepared samples with increasing Y^{3+} concentration.

Prepared samples were also characterized by HR-TEM to get more understanding of the particle size, shape, crystallinity and lattice interplanar distance. Fig. 4 shows the HR-TEM images of Y^{3+} ion-substituted $CoY_xFe_{2-x}O_4$ sintered at 800 °C for x= 0.0 and 0.15. They confirmed that the particles were spherical in shape and agglomerated to some amount due to magnetic dipole interactions occurring within ferrite nanoparticles [17, 18]. The higher reactivity by heat treatment of the prepared samples was a clear sign of
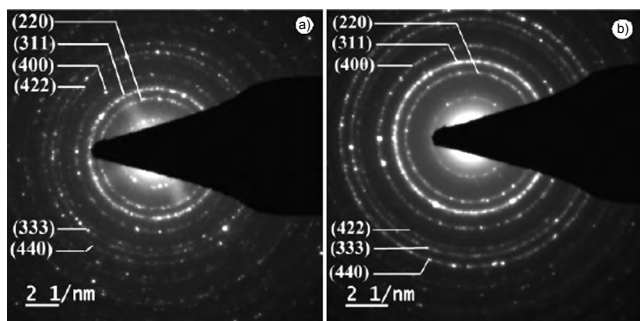
the agglomeration. However, few elongated particles were additionally present in the micrographs as agglomerated particles; the size distribution was challenging to estimate. The pattern which consists of concentric rings and the central bright spot is termed as selected area electron diffraction (SAED) pattern as shown in Fig. 5. The SAED
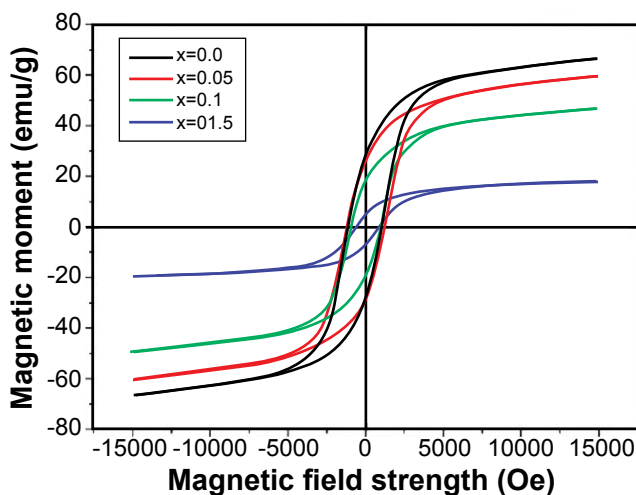

Figure 5: SAED patterns of Y^{3+}-substituted $CoY_xFe_{2-x}O_4$ for: a) x=0.0; and b) x=0.15.
[*Figura 5: Padrões de difração de elétrons de área selecionada (SAED) de amostras de $CoY_xFe_{2-x}O_4$: a) x=0.0; e b) x=0.15.*]

Figure 6: Hysteresis loops of Y^{3+}-substituted $CoY_xFe_{2-x}O_4$ samples.
[*Figura 6: Ciclos de histerese de amostras de $CoY_xFe_{2-x}O_4$.*]

Table II - Magnetic saturation (M_s), coercivity (H_c), remanent magnetization (M_r), magneton number (n_B), and remanence ratio (R) for $CoY_xFe_{2-x}O_4$ samples.
[*Tabela II - Saturação magnética (M_s), coercividade (H_c), remanência (M_r), número de magnéton (nB) e razão de remanência (R) das amostras de $CoY_xFe_{2-x}O_4$.*]

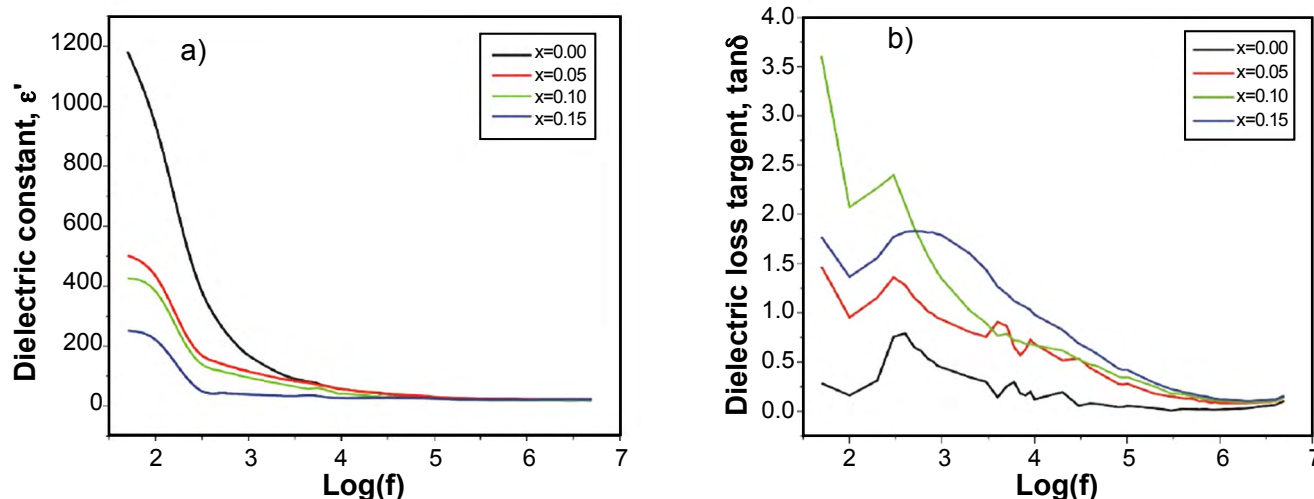| Comp. 'x'	M_s (emu/g)	H_c (Oe)	M_r (emu/g)	n_B	R
0.00	66.61	1168.9	29.02	3.26	0.436
0.05	60.42	1164.7	26.72	3.06	0.442
0.10	46.89	903.8	17.37	2.86	0.370
0.15	17.52	801.9	5.30	2.66	0.302

Figure 7: Variation in dielectric constant (a), and dielectric loss tangent (b) with increasing frequency for $CoY_xFe_{2-x}O_4$ samples (x=0.00, 0.05, 0.10, 0.15).
[*Figura 7: Variação na constante dielétrica (a) e tangente de perda dielétrica (b) com frequência crescente para amostras de $CoY_xFe_{2-x}O_4$ (x=0,00, 0,05, 0,10, 0,15).*]

patterns gave information about the samples, which were polycrystalline in nature. The spotted representation of the diffraction ring was expected due to the high crystallinity of the prepared ferrite nanoparticles. A similar observation has also been reported in the literature [19].

Magnetic properties: Fig. 6 demonstrates the room temperature hysteresis loops (M-H) of Y^{3+} ion-substituted $CoY_xFe_{2-x}O_4$ with a connected magnetic field of 1.5 T. Estimated values of saturation magnetization (M_s), remanent magnetization (M_r), remanence ratio (R), and coercivity (H_c) from the hysteresis loops are given in Table II. It was observed that the saturation magnetization decreased from 66.61 to 17.52 emu/g with increasing Y^{3+} substitution in cobalt ferrite. The decrease in magnetization was due to the substitution of non-magnetic Y^{3+} ions in place of magnetic Fe^{3+} ions. This behavior of M_s can be explained by the site preference of Y^{3+} ion, which may alter the superexchange interactions between tetrahedral A-site and octahedral B-site [20]. As like the decrease in saturation magnetization, the remanent magnetization also reduced from 29.02 to 5.30 emu/g with Y^{3+} ion substitution. Investigations show that the external factors, e.g. porosity, homogeneity, morphology, density, and distribution of cations at lattice sites, considerably affect magnetic parameters [21, 22]. It was observed that the remanence ratio decreased with Y^{3+} ion substitution and the values were below 0.5 which meant that prepared samples had a multi-domain structure [23, 24]. The coercivity fundamentally depends on the magnetocrystalline anisotropy and the particle size. The coercivity of the samples reduced from 1168.9 to 801.9 Oe with enhancing yttrium concentration in the present ferrite system. Similar results are recorded in [25]. Because of the significant spin-orbit coupling, initially, the high value of coercivity begins from the anisotropy of cobalt ions at octahedral B-site. The reduction in magneton number n_B (the saturation magnetization per formula unit in μ_B) is correlated with the decrease in A-B interaction and it is determined using relation discussed elsewhere [26]. As the Bohr magneton number depends directly on the saturation magnetization, reduction in M_s with yttrium addition lowered the Bohr magneton number (Table II).

Electrical properties: Fig. 7a shows the frequency-dependent dielectric constant of $CoY_xFe_{2-x}O_4$ at room temperature. The electrical properties of the ferrite samples generally depend upon the synthesis approach, chemical content, grain size, and sintering temperature. The decrease of dielectric constant with the increase of frequency is expected to occur in ferrite material, which might be because of the interfacial polarization as anticipated by Maxwell-Wagner [27]. The dielectric constant increased with the decrease in the concentration of Y^{3+} ion and the values varied from 251.4 to 1182.4. The dielectric constant was high at low frequency and attained almost constant values at high frequency, which can be explained on the basis of space charge polarization. At low frequency, the space charge polarization builds up due to localized accumulation of charges under the influence of the applied electric field;

therefore, a high value of the dielectric constant is expected at low frequency. As frequency increases, the probability of charge accumulation at the grain boundaries is reduced, thereby reducing the polarization. As a result, dielectric constant decreases with the increase of frequency.

Fig. 7b shows the variation of dielectric loss tangent (tanδ) with frequency. tanδ shows the energy losses within the ferrite material. In the present system, the sample with x=0.15 showed the highest dielectric loss, indicating the favorable condition of hopping between Y^{2+} and Fe^{3+} ions at the octahedral site with the following reaction:

$$Fe^{3+} + Y^{2+} \leftrightarrow Fe^{2+} + Y^{3+} \tag{B}$$

Dielectric loss arises when the polarization creeps with the applied alternating field which is caused by the impurities and imperfections in the crystal. Peaking behavior is explained by the Rezlescu model [28]. According to this model, the peaking behavior occurs when the frequency of charge hopping between the Fe^{2+} and Fe^{3+} absolutely matches with the frequency of the externally applied field. The relation gives the condition for maxima in the dielectric losses of a dielectric material:

$$\omega.\tau = 1 \tag{C}$$

where $\omega=2.\pi.f_{max}$ and τ is the relaxation time. A relation exists between the relaxation time and the jumping probability per unit time, p:

$$\tau = \frac{1}{2.p} \tag{D}$$

Therefore, from Eq. D, it is seen that the maximum occurs when the jumping or hopping frequency of electrons between Fe^{2+} and Fe^{3+} becomes almost equal to the frequency of the applied field. According to the Rezlescu model, the relaxation peaks may be due to the collective contribution of both p and n-type of charge carriers [29]. The electronic exchange between $Fe^{3+} \leftrightarrow Fe^{2+}$ and hole transfer between $Y^{2+} \leftrightarrow Y^{3+}$ in octahedral sites are responsible for such behavior.

CONCLUSIONS

Y^{3+} substitution in the present cobalt ferrite system was successfully achieved by the sol-gel auto-combustion synthesis method. The XRD patterns confirmed the formation of single-phase in pure and substituted cobalt ferrite. The lattice parameters 'a' increased with the yttrium content due to the difference in ionic radii of Fe^{3+} and Y^{3+} ions. The grain size decreased with the yttrium substitution as observed from FE-SEM analysis. The interplanar distance obtained from the HR-TEM images were in good agreement with the XRD indexed planes, confirming the formation of pure and single-phase cubic spinel structure. The saturation magnetization, remanent magnetization, and the coercivity decreased with the substitution of Y^{3+} ion in the present

ferrite system. The dielectric constant (ε') decreased and dielectric loss tangent (tanδ) increased with the substitution of yttrium in the cobalt ferrite composition.

REFERENCES

[1] S. Mornet, S. Vasseur, F. Grasset, E. Duguet, J. Mater. Chem. **14** (2004) 2161.

[2] A.K. Gupta, R.R. Naregalkar, V.D. Vaidya, M. Gupta, Nanomedicine **2**, 1 (2007) 23.

[3] V. Patil, S.E. Shirsath, S. More, S. Shukla, K. Jadhav, J. Alloys Compd. **488** (2009) 199.

[4] R. Kambale, K. Song, Y. Koo, N. Hur, J. Appl. Phys. **110** (2011) 53910.

[5] A. Krell, P. Blank, H. Ma, T. Hutzler, M. Nebelung, J. Am. Ceram. Soc. **86** (2003) 546.

[6] S.E. Shirsath, S.M. Patange, R. Kadam, M. Mane, K. Jadhav, J. Mol. Struct. **1024** (2012) 77.

[7] S. Patange, S.E. Shirsath, B. Toksha, S.S. Jadhav, S. Shukla, K. Jadhav, Appl. Phys. A **95** (2009) 429.

[8] P. Kumara, S.K. Sharma, M. Knobel, M. Singh, J. Alloys Compd. **508** (2010) 115.

[9] S. Singhal, S. Jauhar, J. Singh, K. Chandra, S. Bansal, J. Mol. Struct. **1012** (2012) 182.

[10] S.E. Jacobo, P.G. Bercoff, Ceram. Int. **42** (2016) 7664.

[11] A.M. Pachpinde, M.M. Langade, K.S. Lohar, S.M. Patange, S.E. Shirsath, Chem. Phys. **429** (2014) 20.

[12] R. Pandit, K.K. Sharma, P. Kaur, R.K. Kotnala, J. Shah, R. Kumar, J. Phys. Chem. Solids **75** (2014) 558.

[13] A. Abdeen, J. Magn. Magn. Mater. **192** (1999) 121.

[14] M. Hashim, S. Kumar, B. Koo, S.E. Shirsath, E. Mohammed, J. Shah, R. Kotnala, H. Choi, H. Chung, R. Kumar, J. Alloys Compd. **518** (2012) 11.

[15] U.B. Sontu, V. Yelasani, V.R.R. Musugu, J. Magn. Magn. Mater. **374** (2015) 376.

[16] G. Kumar, S. Sharma, R.K. Kotnala, J. Shah, S.E. Shirsath, K.M. Batoo, M. Singh, J. Mol. Struct. **1051** (2013) 336.

[17] J. Rani, K.L. Yadav, S. Prakash, Mater. Res. Bull. **60** (2014) 367.

[18] G. Aravind, M. Raghasudha, D. Ravinder, M.M. Raja, S.S. Meena, P. Bhatt, M. Hashim, Ceram. Int. **42** (2016) 2941.

[19] I.A. Auwal, A. Baykala, H. Güngüneş, S.E. Shirsath, Ceram. Int. **42** (2016) 3380.

[20] A. Ghasemi, J. Magn. Magn. Mater. **360** (2014) 41.

[21] A. Sharma, R.K. Kotnala, N.S. Negi, Physica B **415** (2013) 97.

[22] R.K. Singh, J. Shah, R.K. Kotnala, Mater. Sci. Eng. B **210** (2016) 64.

[23] P.C.R. Varma, R.S. Manna, D. Banerjee, M.R. Varma, K.G. Suresh, A.K. Ningma, J. Alloys Compd. **453** (2008) 298.

[24] M.M. Rashad, R.M. Mohamed, H. El-Shall, J. Mater. Process. Technol. **198** (2008) 139.

[25] A.V. Raut, R.S. Barkule, D.R. Shengule, K.M. Jadhav, J. Magn. Magn. Mater. **358-359** (2014) 87.

[26] Y. Wu, W. Bensch, J. Alloys Compd. **511** (2012) 35.

[27] Y. Wang, X. Wu, W. Zhang, W. Chen, J. Magn. Magn. Mater. **398** (2016) 90.

[28] M. Eshraghi, P. Kameli, Curr. Appl. Phys. **11** (2011) 476.

[29] P. Chavan, L.R. Naik, P.B. Belavi, G.N. Chavan, R.K. Kotnala, J. Alloys Compd. **694** (2017) 607.